Use of stripping foils in ALPI 4

The study of charge exchange and charge states is an interesting topic in itself, but a number of applications in other areas are also significant. Predictions about charge states and charge-state distributions are often required. One question concerns, for example, the interaction between ions and residual gas along the beam path that leads to a change of the ionic charge and, especially in circular accelerators or storage rings, possibly to losses from the ion beam. Another question is raised by heavy ion linac design and concerns the obtainability of the highest possible charge states of ions behind intermediate strippers in order to optimize further acceleration.

The complex of PIAVE-ALPI is based on the use of an ECR ion source that provides an intense beam of ions with high charge state. In the middle of ALPI it is possible to increase considerably the charge state by means of a Carbon stripper foil obtaining higher final energies as a result. A study of this solution was performed in 2007 to validate the feasibility of the acceleration of a stripped beam, as well as the semi-empirical formulas described in literature and the behavior of different stripper foil thicknesses in terms of obtained average charge states and energy loss.

4.1 Stripping of ions: brief introduction

When heavy ions penetrate through matter, atomic interaction between projectile electrons and target atoms results in considerable fluctuation of the charge state of the ions. In general, the probability of finding an ion in a final charge state q' behind a target depends on five parameters: nuclear charge Z, velocity v, initial charge state q of the ion, target species characterized by the nuclear charge Z_T of target atoms in the case of monatomic targets, and thickness t of the target material.

4.1.1 The physics behind the stripping process

Charge-changing collisions involve a number of different processes (see Fig. 4.1). It is possible to distinguish three mechanisms for fast projectile ions:

1. Coulomb capture. The ion captures one or more (bound) electrons from a target atom into ground or excited states. One particular mode is dielectronic recombination.
2. Radiative capture. The ion captures a free electron or a bound target electron into ground or excited states accompanied by the emission of a photon.
3. Excitation to the continuum. The ion loses one or more electrons, leaving the ion in either ground or excited states.Singly excited ions usually return very fast to the ground state: however, Rydberg states and metastable states may be produced that have relatively long lifetimes. There is a definite chance that ions arc still excited when a subsequent collision takes place. Whenever an ion is left in a multiply excited state. Two further reaction channels must be mentioned that do not produce a direct change of charge: capture to continuum states of the ion and excitation to higher lying unoccupied bound projectile states.

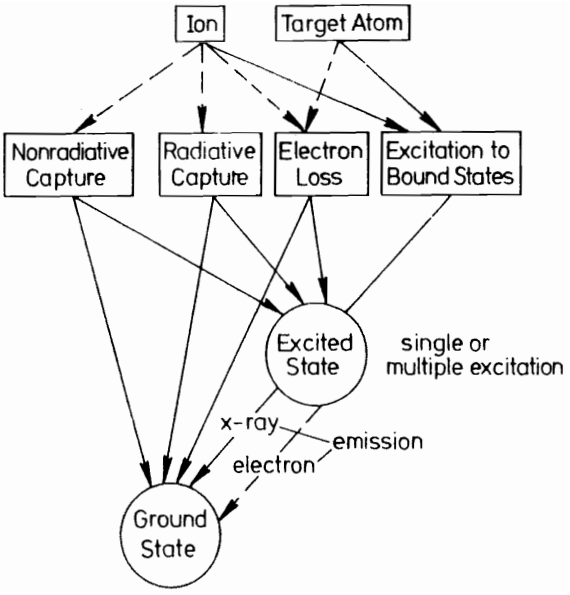

Figure 4.1: Scheme for basic collision-induced ion-atom processes, which lead to a change of the projectile charge state, either directly or via multiply excited states; the broken lines indicate charge-changing processes.

For completeness, it is worth to mention that processes (1)-(3) may also occur to target atoms either directly or in all encounter with neighboring target atoms after recoiling from a collision with a projectile ion.

One must bear in mind that the above processes are not always easily separated from each other and can occur simultaneously in a single Ion-atom encounter. This implies no difficulty either experimentally or theoretically when the collision is sufficiently fast so that the probability P for any of the above processes is small compared to unity. But in very slow collisions, dominant reaction channels can become coupled and the concept of "single collision" with respect to occurrence of a single charge exchange process as specified above may lose significance. The condition for having a fast collision is usually given by $v > v_e$, where v_e, designates the orbital velocity of the transferred electron.

Basic quantities of interest are cross sections $\sigma(q, q')$ for collisions in which the initial charge q has changed to q' when the ion is analyzed. The notation $\sigma(q, q \pm n)$ is also used, where positive and negative signs of n characterize electron loss and capture by the ions, respectively, as well as subscript to distinguish capture (σ_c) and loss (σ_l).

The above processes (1)-(3) depend on the impact parameter b of the collision. Fortunately, dominant contributions to the capture probability $P(b)$ arise from values of b close to the relevant shell radii R, so that Rutherford scattering to large angles is not too important and the ions can be observed mainly in the forward direction.

4.1.2 The charge-state equilibrium

When an ion beam passes with a well-defined velocity v through a target of thickness x (where x is measured in atoms per square centimeter or molecules per square centimeter) the charge-state composition of the beam will vary because of capture and loss events and for each value of x certain relative charge-state populations $P_q(x)$ will be observed.

These charge-state fractions $P_q(x)$ obey a system of linear coupled differential equations,

$$\frac{dP_q(x)}{dx} = \sum_{q' \neq q} \Big[\sigma(q', q)P_{q'}(x) - \sigma(q, q')P_q(x)\Big], \tag{4.1}$$

where q and q' extend over the range of possible charge states.

For convenience, the fractions P are normalized by $\sum_q P_q = 1$. For light ions only a few charge states are dominant whereas heavy ions exhibit mostly broad distributions $P(q)$ and a very

large number of fractions must be considered. It is important to note that Eq. 4.1 is valid only as long as the cross sections a are constant and do not depend on x; otherwise residual ion excitation is effective.

The incident charge fraction decreases at the expense of neighboring fractions. In the absence of cross-section anomalies each component $P_q(x)$ exhibits at most one extremum. When x becomes sufficiently large, the fractions do not change further and equilibrium is reached. Significance of non-equilibrium distributions lies in their usefulness for determination of cross sections.

Charge-state equilibrium is attained for a certain minimum target thickness t_∞, which depends on the absolute magnitude of cross sections and, to some extent, on the initial charge distribution $P_q(0)$. Equilibrium charge-state fractions, which will be denoted by P_q, are independent of the initial distribution $P_q(0)$ and reflect ratios of cross sections. In most collision systems independence of P_q on further increase of t is easily measurable, but energy loss and scattering may prevent clear-cut observations of that kind [1].

If one assumes that only single electrons are captured or lost, i.e. when $|q' - q| = 1$, Eq. 4.1 provides a simple relation between fractions and cross sections,

$$\frac{P(q)}{P(q+1)} = \frac{\sigma_c(q+1)}{\sigma_l(q)}. \tag{4.2}$$

This equation is indeed useful for very light targets where multiple electron capture and loss is generally of little importance. The cross section σ_c and σ_l have been calculated theoretically by several authors [2]. Electron capture dominates at low v (E < 0.5 MeV/A) when the velocity is comparable to the orbital velocity of the electrons. At higher energies (E > 2 MeV/A), electron loss becomes the dominant featire. When a complete set of cross sections $\sigma(q, q')$ is known, all corresponding fractions $P(q)$ can be directly calculated without integration of Eq. 4.1.

4.1.3 Experimental data

It is useful to define three parameters for both the non-equilibrium and equilibrium charge distributions, namely the average charge $\bar{q}$, the width d and the skewness s:

$$\bar{q} = \sum_q q\, P(q), \tag{4.3}$$

$$d = \sqrt{\sum_q (q - \bar{q}_\infty)^2 P(q)}, \tag{4.4}$$

$$s = \sum_q \frac{(q - \bar{q}_\infty)^3 P(q)}{d^3}. \tag{4.5}$$

Equilibrium distributions may be represented by a Gaussian distribution,

$$P(q) = \frac{1}{d\sqrt{2\pi}} \exp\left(-\frac{(q - \bar{q}_\infty)^2}{2d^2}\right), \tag{4.6}$$

where $\bar{q}_\infty$ is the average charge for the equilibrium distribution and $s = 0$.

Most of the data on charge states and cross sections has been accumulated by utilizing tandem Van de Graaff accelerators. In the 60's many experiments were carried out to obtain an extensive database of charge states distributions for a large variety of ions, strippers (both gaseous and solid) and energies: the main purpose was the optimization of the stripper stations inside the tandem accelerators itself, to predict with the highest accuracy the most probable charge state for a given stripper density, that is the highest final energy with the minimum energy straggling, which happens for a foil thickness just above t_∞. In fact $\bar{q}$ begins to decrease for solid foils as one goes significantly above t_∞ because of energy loss effects.

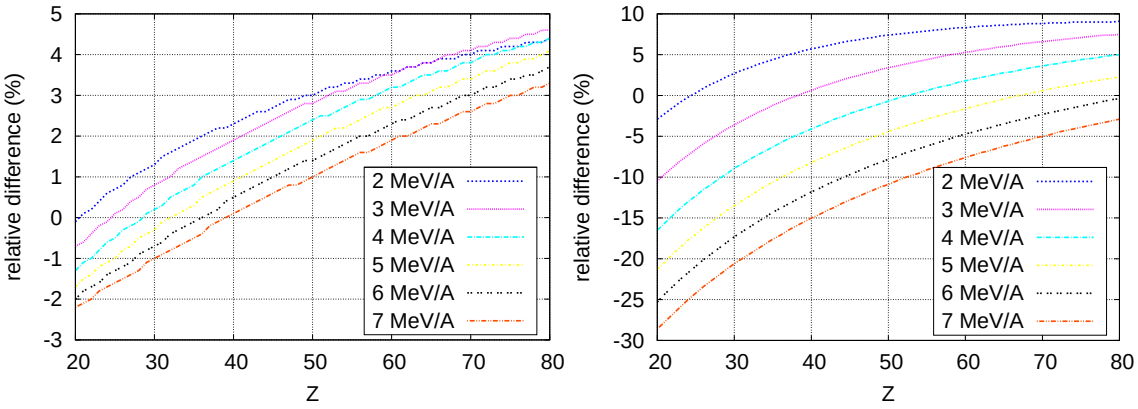

(a) Relative difference between $\bar{q}_\infty$ values.

(b) Relative difference between d values.

Figure 4.2: Comparison between the two semi-empirical formulas Eq. 4.7 and Eq. 4.8.

Semi-empirical formulas

Among the semi-empirical formulas derived by different authors and organized by stripper material, Z of the impinging ions and energy range, the best regarded and used for Carbon stripper foils, medium/high Z and few MeV/A are the ones by Nikolaev and Dmitriev (in [3], 1968):

$$\bar{q}_\infty(Z,v)_{\mathrm{N\&D}} = Z\cdot\left(1+2.29\cdot\left(Z^{-0.45}\frac{v}{v_0}\right)^{-5/3}\right)^{-3/5} \qquad \text{with} \qquad d_{\mathrm{N\&D}} = \frac{1}{2}\sqrt{\bar{q}_\infty\left(1-\frac{\bar{q}_\infty}{Z}\right)^{5/3}}, \quad (4.7)$$

and by Betz (in [4], 1983):

$$\bar{q}_\infty(Z,v)_{\mathrm{Betz}} = Z\cdot\left[1-1.041\cdot\exp\left(-0.851\cdot Z^{-0.432}\left(\frac{v}{v_0}\right)^{0.847}\right)\right] \qquad \text{with} \qquad d_{\mathrm{Betz}} = 0.27\,Z^{\frac{1}{2}}, \quad (4.8)$$

where v_0 is the velocity of the electron in the orbital $\lambda = 1$ ($v_0 = e^2/h = 2.188\times10^6$ m/s).

As shown in Fig. 4.5, the two semi-empirical formulas for $\bar{q}_\infty$ differ by only few percents for a large range of Z and energy, i.e. 2 unit charge for the heaviest ions. Larger differences come from the d values and they affect inversely the $\bar{q}_\infty$ probability ($P_{\bar{q}_\infty} = 1/(d\sqrt{2\pi})$): as the energy becomes larger the relative difference goes up to 30%, but it is not a real problem of the purpose which the formulas will be used for, since the current nuclear-community interest lies more on the high Z nuclei for such energies (see the Introduction for more details).

Both formulas show a smooth trend and come from averages which do not include the effects of electronic shells. The shell effects, as extensively shown in [5], can have a large effect on both the average charge state and width, particularly for very heavy ions, where the difference in $\bar{q}_\infty$ can be as large as five charge states. Attempts have been made to calculate correction factors for shell effects; however these corrections are very dependent on both the ion and the energy and extrapolation is difficult.

Effects on beam energy through a solid stripper

The energy loss of an ion trough a solid stripper could be easily calculated with SRIM [6]. The program uses principally fittings of a large database of experimental data, but it does not take into account the actual charge of the impinging ion and the process of stripping which takes place in the media. In [7] rigorous expressions have been derived for the mean energy loss of ions penetrating through foils, specified into entrance and exit charge states. These expressions allow

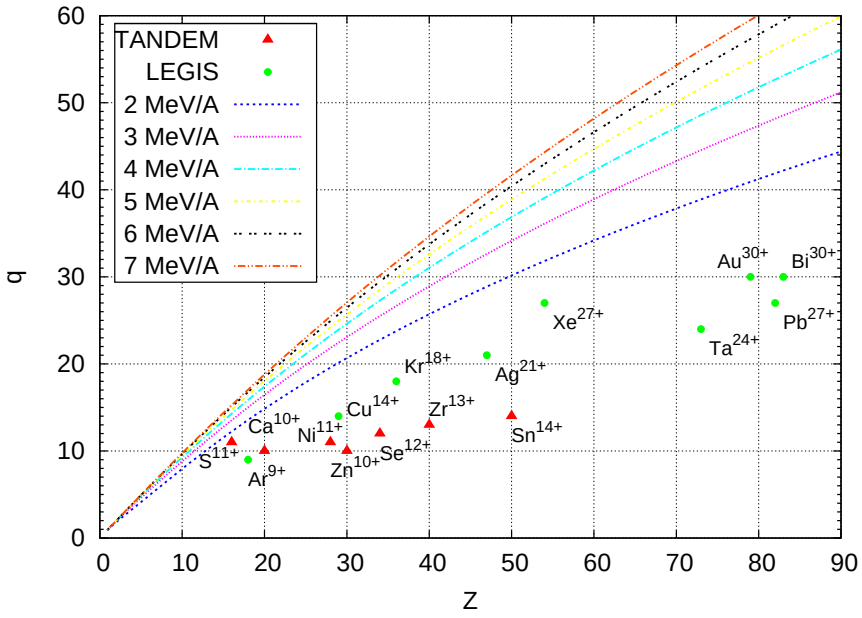

Figure 4.3: Most probable charge states after stripping as a function of Z and energy compared to some examples of available ions from LEGIS (see Tab. 3.2) or out of TANDEM injector.

extraction of partial stopping cross sections and charge-exchange cross sections in solids from measured energy losses versus foil thickness. More recently, in [8], this approach was combined with Monte Carlo simulations.

Concerning the energy straggling, in [9] a formula was presented which relates this effect to the characteristics of both the ion (Z, A and E) and the stripper (Z_s and A_s):

$$\frac{\delta E}{E} = 0.5 \cdot 10^{-3} \cdot \frac{1.866 + 1.57 \cdot \log(E)}{E} \cdot \frac{Z}{A} \cdot \sqrt{\frac{Z_s}{A_s} \cdot t}, \tag{4.9}$$

where E is here expressed in [MeV/A] and t in [$\mu g/cm^2$]. The uncertainty on the predictions of this formula comes from the local inhomogeneity of the media, which is inherent in the process of stripper fabrication but is also caused by the ion bombardment itself.

4.2 Experience with stripping Carbon foils in ALPI

In January 2007 it was decided to place a stripper station in the center of the last low-energy branch period, at the both transverse and longitudinal focal point. In fact the energy straggling affects both the longitudinal and transverse plane: taking into account that this effect acts only on the velocity distributions, a strong focusing is the only way to minimize the undesired emittance growths. Hence, the diagnostics box DO4 was modified to held the device. The overall scheme is shown in Fig. 4.4.

The position of the Carbon stripper foil along the accelerator was chosen to optimize the overall energy gain: the energy before the stripping is about 3 MeV/A (see Tab. 1.1), enough to enhance the charge state by 50% for the medium/high mass ions (see Fig. 4.3), and the remaining accelerating voltage is 2/3 of the total voltage. This means that the final energy of the stripped beam is 20 ~ 30% higher than the unstripped one. Moreover, at these energies the energy spread increase due to the stripping is about 0.05%, one order of magnitude less than the typical energy spread of the beam at the end of the ALPI low-energy branch.

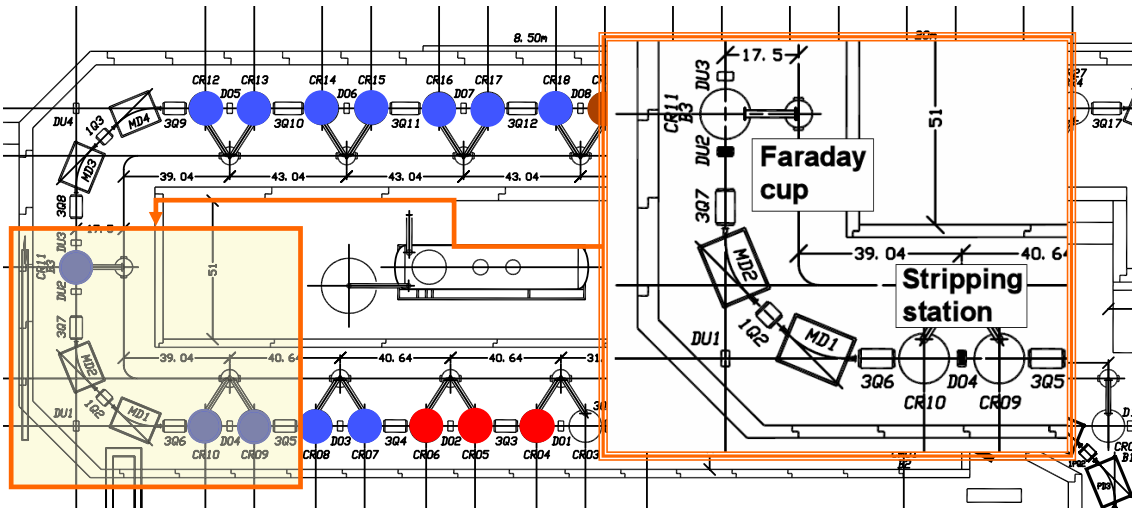

Figure 4.4: ALPI layout around the stripper station. The beam coming from either TANDEM or PIAVE injector is accelerated by the low-β (in red) and the first three medium-β (in blue) cryostats, it is focalized in the diagnostic box D04, stripped and then selected by the two dipoles MD1 and MD2. Once the most probable charge state is chosen, the beam is accelerated by the remaining cryostats (high-β in brown).

4.2.1 The experimental set-up

The stripper station foresees a carousel equipped with a hundred stripper foil of various thickness values (5-10-20-50 μg/cm^2) preceded by a collimator, which ensures a proper beam focusing at the foil plane. The system is remote-controlled via PC. Downstream the stripper station the beam is focalized by 3Q6 triplet and bent by MD1 and MD2, whose magnetic field is measured by a Tesla-meter with a precision of $1/10^6$. The beam passes through 3Q7 triplet (set to off) and is then monitored relatively to its position and current in the diagnostics box DU2, in the middle of the U-bend. This way, the first half of the U-bend acts as a spectrometer. The experimental procedure consists in recording dipole field and current of both the collimated unstripped beam and of the different stripped charge states, which are selected by the dipoles. The Dispersion function in DU2 is about 5 m (see Fig. 4.9), which gives enough separation to the charge states: considering a beam with an energy spread of ±0.5% and an RMS emittance of 0.15 mm.mrad norm., the spot size on DU2 grills would be around 5 cm, 2.5 ($\Delta B/B = \Delta q/q = 1/40$) to 10 ($\Delta q/q = 1/10$) times smaller than the distance between to adjacent charge-states beams. The procedure, which takes about ten mins, is then repeated for the different foil thicknesses. The drawback of this solution is that the charge-state distributions can not be recorded at the same time, implying some problems in the data normalization.

4.2.2 Data analysis

If $i(q)$ is the beam current per unit charge of ions having charge state q after being stripped, the charge state fraction is defined by $P(q) = i(q)/\sum_q i(q)$. Figure 4.5 shows the evolution of the charge state fractions for ^{90}Zr, ^{48}Ca (from Tandem) and ^{136}Xe, ^{36}Ar (from PIAVE) as a function of the carbon target thickness t. As the thickness is increased, the $P(q)$ curve moves towards higher charge states. The equilibrium thickness t_∞ is reached when the average charge state $\bar{q} = \sum_q P(q)$ stops raising.

In Tab. 4.1 the results of the charge-states distribution analysis are shown: for all the beams except ^{136}Xe it is clear that the equilibrium thickness is reached for $t < 50$ μg/cm^2. The higher order parameters d and s are too sensitive to the data normalization and give no information.

Table 4.1: Stripping probability analysis as a function of target thickness. The parameters $\bar{q}$, d and s are calculated using Eq. 4.3, Eq. 4.4 and Eq. 4.5 respectively.

ion	Z	E (MeV/A)	5 μg/cm^2			10 μg/cm^2			20 μg/cm^2			50 μg/cm^2		
			$\bar{q}$	d	s	$\bar{q}$	d	s	$\bar{q}$	d	s	$\bar{q}$	d	s
$^{136}Xe^{23+}$	54	2.475	30.0	2.1	4							33.9	1.6	-2
$^{90}Zr^{13+}$	40	2.614	25.5	1.9	6	26.0	1.8	7				27.9	1.7	5
$^{36}Ar^{8+}$	18	3.206	14.5	1.0	-1	14.4	1.0	1	14.9	0.9	1	15.0	0.9	0
$^{48}Ca^{9+}$	20	3.487	15.4	1.2	-4	15.8	0.8	-4	16.6	0.7	1	16.9	0.5	8

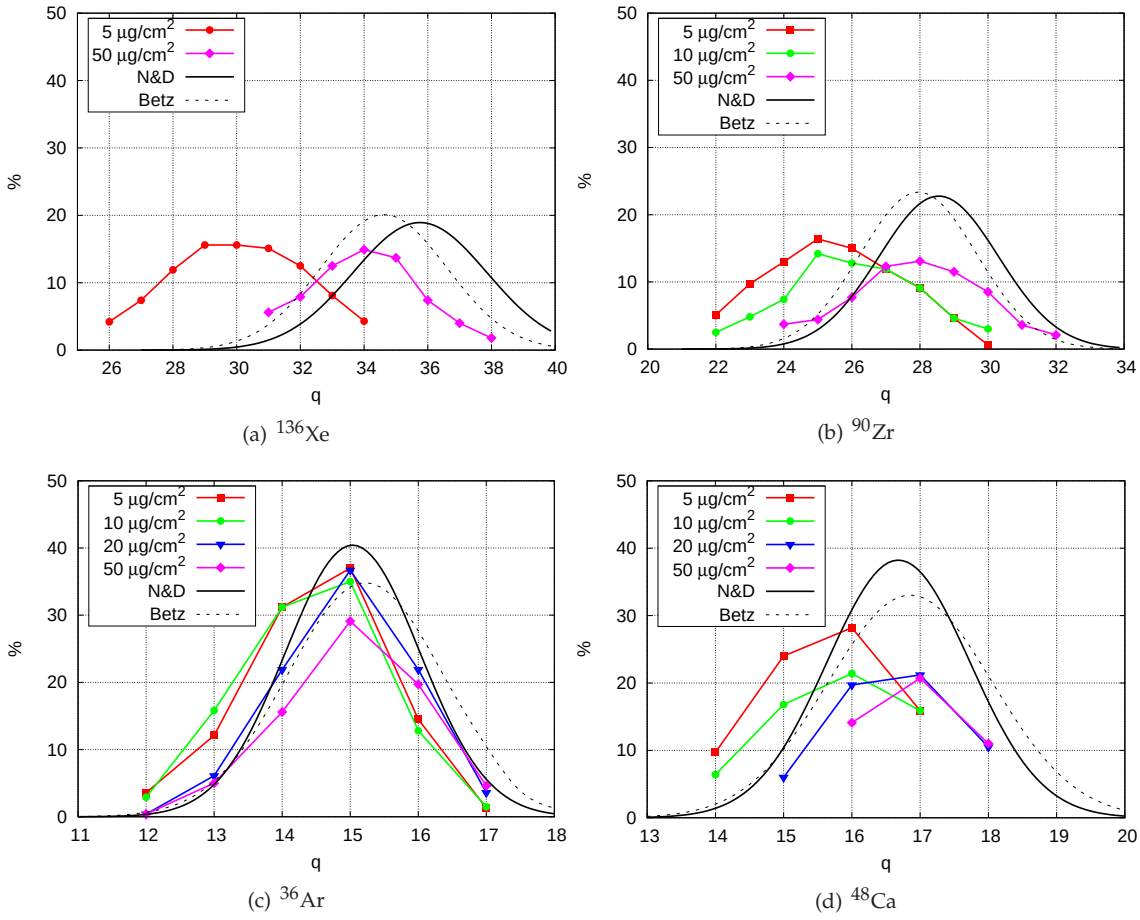

(a) ^{136}Xe (b) ^{90}Zr

(c) ^{36}Ar (d) ^{48}Ca

Figure 4.5: Stripping probability $P(q)$ as a function of target thickness. The data are normalized on the total beam current before stripping. N&D (Eq. 4.7) and Betz (Eq. 4.8) predictions are added as comparison.

Table 4.2: Average charge after stripping. The experimental results, both maximum value and the the value coming from the data fit, and the predictions are compared.

ion	Z	E (MeV/A)	experimental $\bar{q}_\infty$		theoretical $\bar{q}_\infty$		t_∞
			max. data	by fit	N&D	Betz	(μg/cm^2)
$^{136}Xe^{23+}$	54	2.475	33.9 ± 0.4	33.9	35.8	34.6	24
$^{90}Zr^{13+}$	40	2.614	27.9 ± 0.7	27.2 ± 0.7	28.5	28	13 ± 3
$^{36}Ar^{8+}$	18	3.206	15.0 ± 0.4	14.8 ± 0.1	15.0	15.2	9 ± 3
$^{48}Ca^{9+}$	20	3.487	16.9 ± 0.3	16.6 ± 0.2	16.7	16.9	15 ± 3

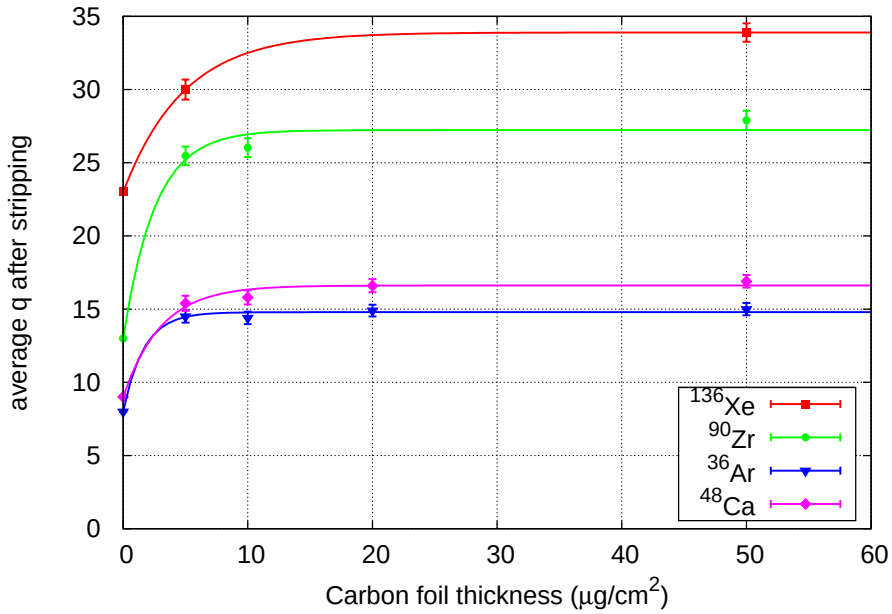

Figure 4.6: Average charge after stripping as a function of the target thickness. Fit by Eq. 4.10.

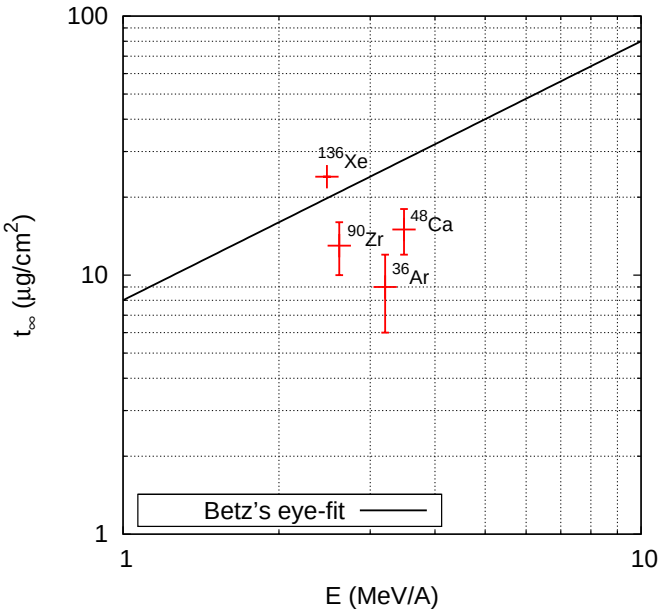

Figure 4.7: Comparison between the experimental equilibrium thickness and Betz's eye-fit function [4]: $t_\infty[\mu g/cm^2] = 8 \cdot E$ [MeV/A].

Table 4.3: Beam energy loss as function of target thickness. The data come from the fit by Eq. 4.11 and are compared to the values calculated via SRIM [6].

ion	Z	E (MeV/A)	ΔE/Δx (keV/μg/cm^2)		δE (%)
			by fit	by SRIM	
$^{136}Xe^{23+}$	54	2.475	78.8	82.9	0.86
$^{90}Zr^{13+}$	40	2.614	62 ± 6	58.1	0.46 ± 0.08
$^{36}Ar^{8+}$	18	3.206	18 ± 3	19.4	0.77 ± 0.05
$^{48}Ca^{9+}$	20	3.487	22 ± 6	22.7	0.21 ± 0.15

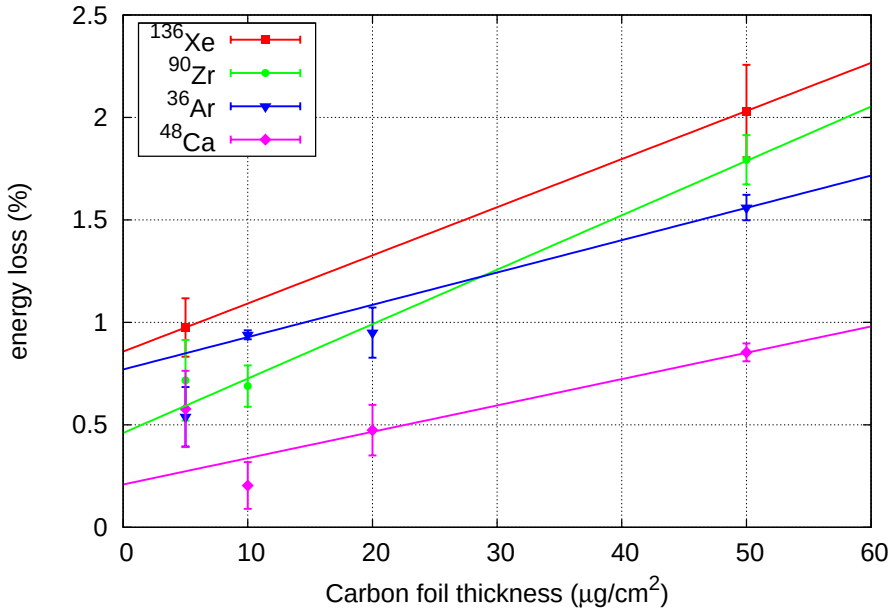

Figure 4.8: Beam energy loss as a function of the target thickness. Fit by Eq. 4.11.

Equilibrium distribution

The $\bar{q}$ as function of t (Fig. 4.6) can be fitted by

$$\bar{q}(t) = q_0 + (\bar{q}_\infty - q_0)\ e^{-\frac{t}{k}}, \tag{4.10}$$

where q_0 is the charge of the beam before stripping and $\bar{q}_\infty$ is the most probable charge state for t_∞. This formula, already used in [10], is misleading because the beam loses part of its energy as it passes through the foil, resulting in a drop of $\bar{q}$ for $t >> t_\infty$. Nevertheless, for low thickness, it is very useful since it is possible to obtain the $\bar{q}_\infty$ in a simple way. From the comparison in Tab. 4.2 the predictions by the semi-empirical formulas seem to be in good agreement with both the maximum $\bar{q}$ of the data distributions and the $\bar{q}_\infty$ from this fit.

From the Eq. 4.10 it also possible to obtain an estimate of the t_∞: assuming that $t_\infty \simeq 5\ k$, the results are reported in Tab. 4.2. The statistical errors of these value are greater than 20% and could be reduced only if a much larger sample of thicknesses across 5 μg/cm^2 were analyzed. A large collection of t_∞ data from various stripping experiments was collected by Betz in [4]: he proposed a simple eye-fitting function for all the data, namely $t_\infty[\mu g/cm^2] = 8 \cdot E$ [MeV/A]. In Fig. 4.7 this formula is compared with the experimental values just described.

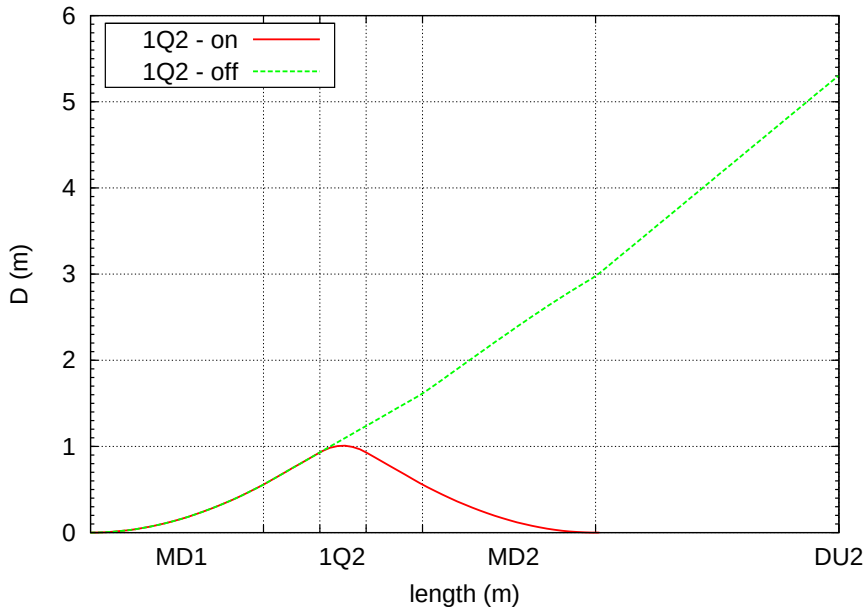

Figure 4.9: Dispersion function for the first half of the U-bend. The dispersion inside 1Q2 singlet is about 1 m and reaches 5.3 m at DU2.

Energy loss

Concerning the beam energy loss through the stripper, the data in Fig. 4.8 are linearly fitted by

$$\Delta E(t) = \delta E + \Delta E/\Delta x \cdot t, \tag{4.11}$$

where $\Delta E/\Delta x$ is the stopping power and δE is the error on the beam energy before stripping (see Tab. 4.3). For all the four beams, the former perfectly matches the value calculated via SRIM program [6]. On the contrary, the latter is not compatible with zero: a systematic error was clearly committed in the energy measurement, probably due to a slight misalignment of the beam line.

4.2.3 Beam acceleration

^{136}**Xe**$^{30+}$ was easily transported to the experiment: the final energy reached 1.1 GeV (8.1 MeV/A), 20% more of the energy of the unstripped beam (923 MeV). By simulations (Fig. 4.10) the effect of the stripper on the energy spread of the beam is almost negligible, but the transmission in the ALPI high-energy branch was limited to 50%, compared to the 90% obtained by PARMELA (see Fig. 4.11). Thanks to the high current provided by the ECRIS, the beam current on target was yet greater than 1 pnA.

^{90}**Zr**$^{28+}$ was transported only up to half of the high-energy branch. Due to the low current of the selected charge state (< 1 pnA), the cavity setting was extremely difficult and the right synchronous phase setting could not be guaranteed.

^{36}**Ar**$^{15+}$ was transported to the experiment with some troubles due the failure of the last cryostat before the stripper station (CR09) along with the second cryostat after the U-bend (CR13). The final energy reached 450 MeV, whereas the energy without stripping was 300 MeV. The lack of the four cavities before the stripper did not allow to focus longitudinally the beam at the foil plain (see Fig. 4.10) and the transmission of the high-energy branch was extremely low (20%). The complete simulation set of Fig. 4.12 shows a similar result, with losses all along the accelerator.

^{48}**Ca**$^{17+}$ was not transported since the current was too low for the synchronous phase setting.

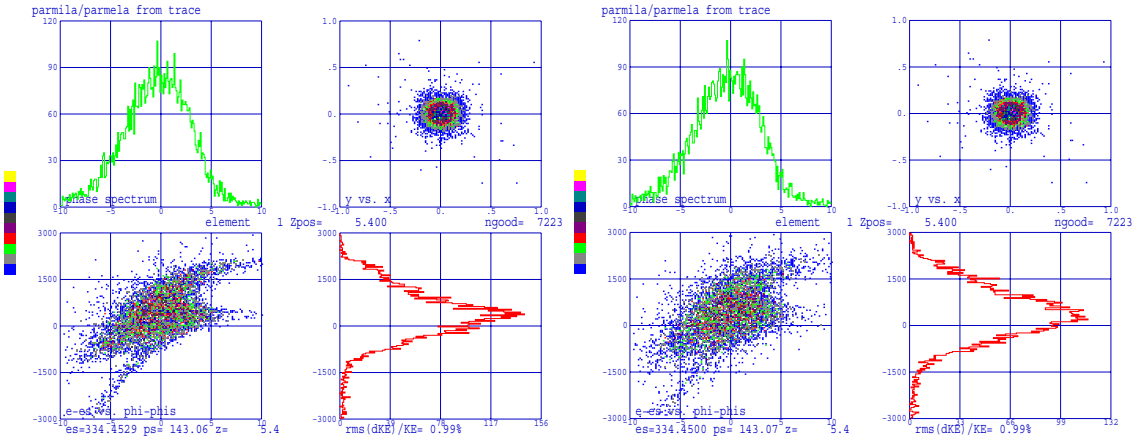

(a) ^{136}Xe before the stripper.

(b) ^{136}Xe after the stripper.

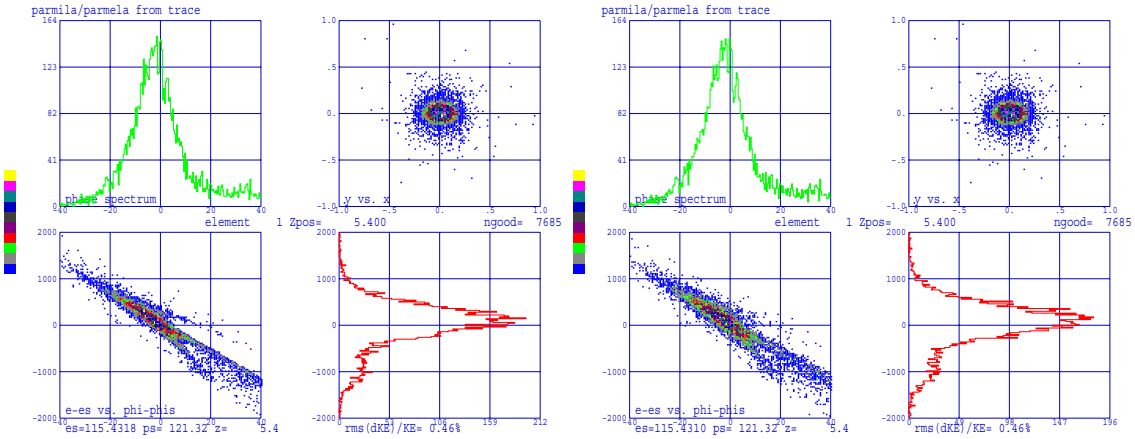

(c) ^{36}Ar Before the stripper.

(d) ^{36}Ar after the stripper.

Figure 4.10: Simulations of ^{136}Xe and ^{36}Ar passing through the stripper. The energy straggling is limited to ±0.045% for ^{136}Xe and ±0.033% for ^{36}Ar and the effect is almost negligible.

4.2.4 Conclusions

All the charge-states distribution were in agreement with the theoretical predictions. Concerning the acceleration, it was completed only for the beams injected by PIAVE thanks to the high current provided by the ECRIS ion source. The low-energy branch beam dynamics seems to be very critical to obtain a strong longitudinal focusing at the foil plane and must be experimentally optimized.

The transport of more than one charge state along the accelerator is impossible at these energies (i.e. charge states). The Dispersion function at 1Q2, the singlet of the first half of ALPI U-bend, is about 1 m (see Fig. 4.9): since the bore radius is 2.5 cm, only the beams with $\Delta B/B = \Delta q/q < 2.5\%$ will completely survive. This means that only the beams with $\bar{q}_\infty > 40$ will pass the U-bend with the two neighboring charge states uncut. From Fig. 4.3, these charge states are available for medium Z ions (like Xe) only at energies at stripping greater than 5 MeV/A.

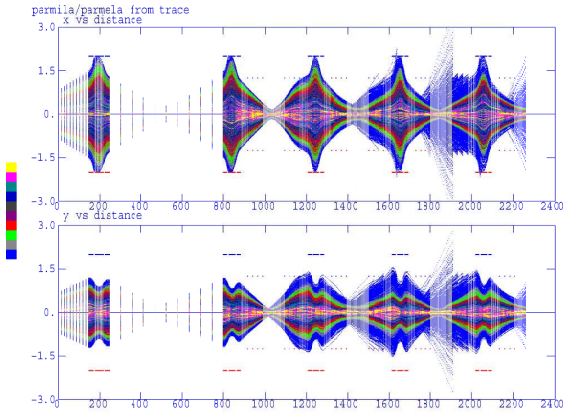

(a) $^{136}Xe^{23+}$ transv. envelopes before stripping.

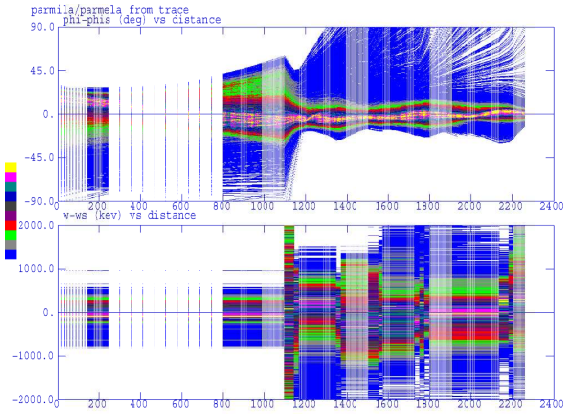

(b) $^{136}Xe^{23+}$ long. envelopes before stripping.

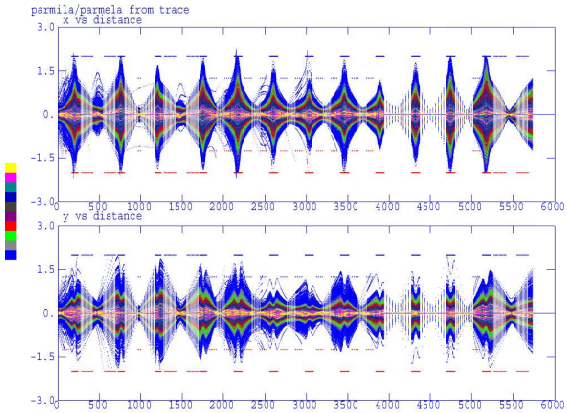

(c) $^{136}Xe^{30+}$ transv. envelopes.

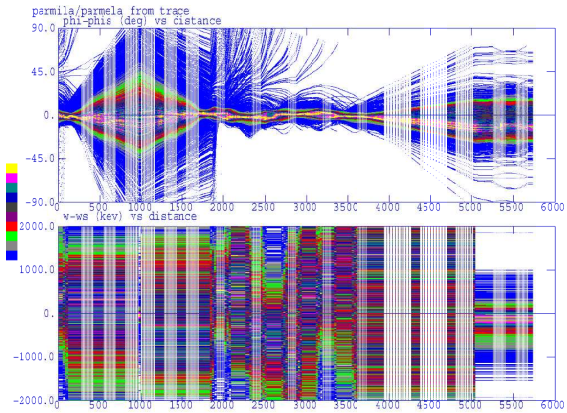

(d) $^{136}Xe^{30+}$ long. envelopes.

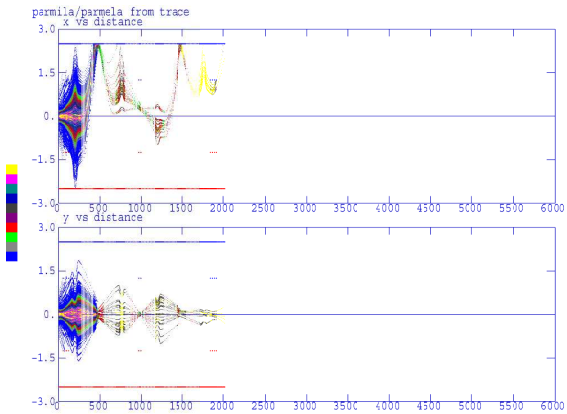

(e) $^{136}Xe^{29+}$ transv. envelopes.

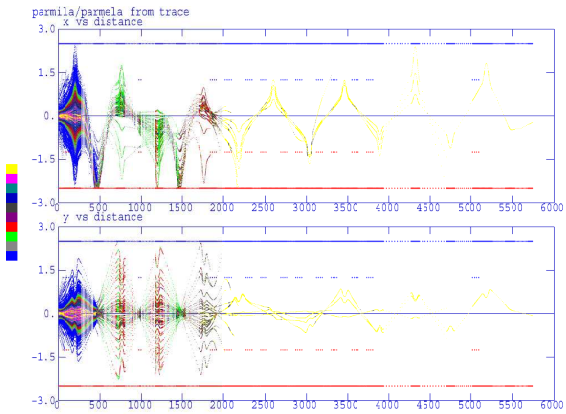

(f) $^{136}Xe^{31+}$ transv. envelopes.

Figure 4.11: ^{136}Xe acceleration beam dynamics including stripper. Simulated via PARMELA, 10k macroparticles. 90% of 30+, 0% of 29+ and 1% of 31+ are accelerated up to the end of the high-energy branch.

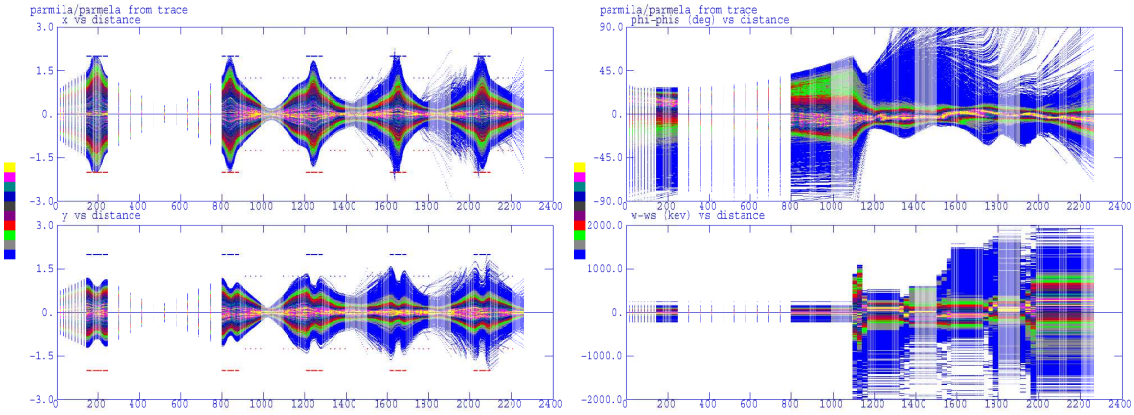

(a) $^{36}Ar^{8+}$ transv. envelopes before stripping.

(b) $^{36}Ar^{8+}$ long. envelopes before stripping.

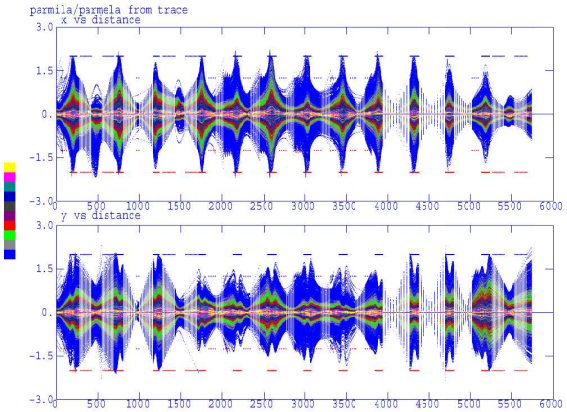

(c) $^{36}Ar^{15+}$ transv. envelopes.

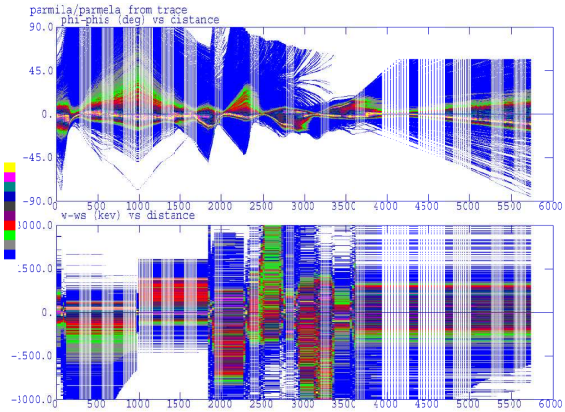

(d) $^{36}Ar^{15+}$ long. envelopes.

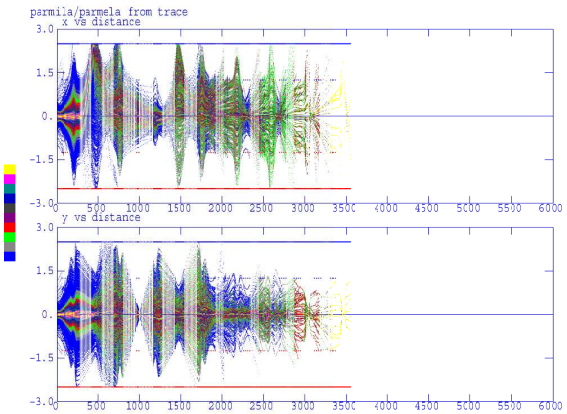

(e) $^{36}Ar^{14+}$ transv. envelopes.

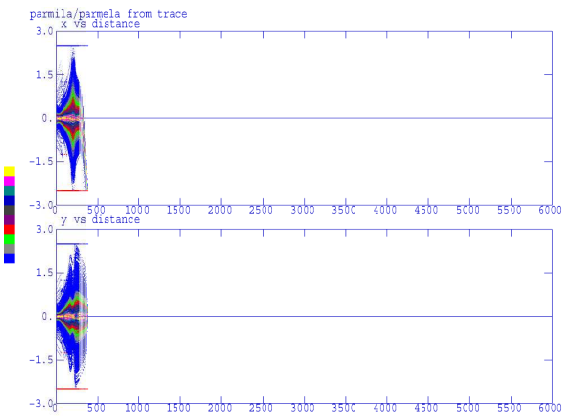

(f) $^{36}Ar^{16+}$ transv. envelopes.

Figure 4.12: ^{36}Ar acceleration beam dynamics including stripper. Simulated via PARMELA, 10k macroparticles. 50% of 15+, 0% of 14+ and 0% of 16+ are accelerated up to the end of the high-energy branch.

Bibliography

[1] C. D. Moak, L. B. Bridwell, H. A. Scott, G. D. Alton, C. M. Jones, P. D. Miller, R. O. Sayer, Q. C. Kessel, and A. Antar, "Absolute charge state yields of 20 MeV ^{127}I Ions emerging from a gas stripper," *Nuclear Instruments and Methods*, vol. 150, pp. 529–535, 1978.

[2] H. D. Betz, "Charge States and Charge-Changing Cross Sections of Fast Heavy Ions Penetrating Through Gaseous and Solid Media," *Rev. Mod. Phys.*, vol. 44, pp. 465–539, Jul 1972.

[3] V. S. Nikolaev and I. S. Dmitriev, "On the equilibrium charge distribution in heavy element ion beams," *Physics Letters*, vol. 28A, pp. 277–278, December 1968.

[4] H. D. Betz, "Heavy Ion Charge States," in *Applied Atomic Collision Physics* (S. Datz, ed.), p. 1, Academic Press, 1983.

[5] K. Shima, N. Kuno, and M. Yamanouchi, "Systematics of equilibrium charge distributions of ions passing through a carbon foil over the ranges Z=4–92 and E=0.02–6 MeV/u," *Phys. Rev. A*, vol. 40, pp. 3557–3570, Oct 1989.

[6] J. F. Ziegler, J. P. Biersack, and U. Littmark, "The Stopping and Range of Ions in Solids," in *Stopping and Ranges of Ions in Matter*, vol. 1, New York: Pergamon Press, 1984.

[7] P. Sigmund, "Analysis of charge-dependent stopping of swift ions," *Phys. Rev. A*, vol. 50, pp. 3197–3201, Oct 1994.

[8] B. Rosner, S. Datz, W. Wu, N. L. Jones, D. R. Schultz, and C. O. Reinhold, "Charge-state dependence of energy loss in random solids," *Phys. Rev. A*, vol. 57, pp. 2737–2741, Apr 1998.

[9] E. Baron and C. Ricaud, "Beam foil interaction studies for the future stripper of GANIL," in *Proceedings of EPAC1988*, pp. 839–841, 1988.

[10] E. Baron and B. Delaunay, "Stripping of high-energy Krypton ions by various solid materials," *Phys. Rev. A*, vol. 12, pp. 40–44, Jul 1975.